PHYSICAL REVIEW B **86**, 104413 (2012)

Effects of Al substitution on the multiferroic properties of $TbMnO_3$

Vera Cuartero,[1,2] Javier Blasco,[1,*] J. Alberto Rodríguez-Velamazán,[1,3] Joaquín García,[1] Gloria Subías,[1] Clemens Ritter,[3] Jolanta Stankiewicz,[1] and Laura Canadillas-Delgado[1,†]

[1]*Instituto de Ciencia de Materiales de Aragón, Departamento de Física de la Materia Condensada, CSIC-Universidad de Zaragoza, C/ Pedro Cerbuna 12, 50009 Zaragoza, Spain*

[2]*ALBA Synchrotron/CELLS, Cerdanyola del Vallès, 08290, Spain*

[3]*Institut Laue-Langevin, Boîte Postale 156, 38042 Grenoble Cèdex 9, France*

(Received 7 June 2012; published 10 September 2012)

The effect of a small substitution of Mn with Al in $TbMnO_3$ has been studied. We report results of heat capacity, magnetization, and dielectric constant studies in $TbMn_{1-x}Al_xO_3$ compounds ($x \leqslant 0.1$). Al has the same valence as substituted Mn but is nonmagnetic and its small size gives rise to microstructural strain which affects the multiferroic properties of the parent compound. Long-range antiferromagnetic ordering is observed in all compounds but the transition temperature decreases as the Al content increases. $TbMn_{0.95}Al_{0.05}O_3$ exhibits a ferroelectric phase transition which is absent in $TbMn_{0.9}Al_{0.1}O_3$. The dielectric constant of the latter compound reveals a relaxor behavior suggesting the presence of nanosize polar domains for this compound. A neutron diffraction study on a single crystal of $TbMn_{0.9}Al_{0.1}O_3$ reveals that Mn shows a sinusoidal incommensurate ordering down to low temperature. Tb moments exhibit an incommensurate short-range ordering but the application of a magnetic field leads to metamagnetic transitions. In particular, a field parallel to the b axis induces a commensurate long-range ordering of Tb of type C_xF_y. The magnetic field also affects the magnetic structure of Mn^{3+} moments at low temperature which develop an incommensurate cycloid ordering in the ab plane. This result suggests that dilution of a magnetic multiferroic with a small nonmagnetic atom might yield materials with a relaxor to ferroelectric transition driven by a magnetic field.

DOI: 10.1103/PhysRevB.86.104413 PACS number(s): 75.85.+t, 61.05.fm, 61.05.cp, 64.70.Rh

I. INTRODUCTION

The study of $TbMnO_3$ has revealed new fascinating properties.[1–3] This compound belongs to the family of magnetoelectric multiferroics,[4] and upon cooling it undergoes three consecutive transitions at 41, 27, and 8 K.[1] At $T_{N1} \sim 41$ K, Mn moments order antiferromagnetically (A-type-like ordering) with an incommensurate modulation described by a wave vector of $\mathbf{k}_{Mn} = (0, q_{Mn}, 0)$, q_{Mn} being 0.295 at T_{N1}.[5] The moments are oriented along the b axis with a sinusoidal modulation of its magnitude.[5,6] At $T_f \sim 27$ K, a spontaneous polarization parallel to the c axis ($\mathbf{P} \parallel \mathbf{c}$) occurs, indicative of a ferroelectric phase transition.[1] This transition is coupled to a magnetic spin rearrangement of the Mn moments which form an elliptical spiral in the bc plane below T_f, the so-called cycloid ordering.[7] Accordingly, q_{Mn} decreases between T_{N1} and T_f to a value of ~0.276 at T_f, and remains practically constant upon further cooling.[8] This behavior resembles a lock-in transition with the magnetic wave vector $\mathbf{k}_{Mn}$ adopting a constant value at T_f.[1,8] At $T_{N2} \sim 8$ K, the Tb magnetic moments begin to order with a different propagation vector $\mathbf{k}_{Tb} = (0, q_{Tb}, 0)$ and $q_{Tb} \sim 0.42$.[8] It is thought that the magnetically ordered Mn sublattice polarizes the rare earth (R) spins by the direct exchange interaction, $J_{Mn\text{-}R}$, and it plays an important role in the developing of ferroelectricity. The strength of this interaction depends on R. It is very strong for R = Ho giving rise to the same ordering periodicity for Mn and Ho moments below 22 K ($q_{Mn} = q_{Ho} = 1/2$).[9] This coupling is very weak for R = Dy ($q_{Mn} \neq q_{Dy} = 1/2$),[10] and intermediate for $TbMnO_3$ as reflected by the relationship[11] $3q_{Tb} - q_{Mn} \approx 1$.

The most striking property of $TbMnO_3$ is the flopping of $\mathbf{P}$ by applying a magnetic field parallel to either the a or b axis.[12] This transition seems to be coupled to a metamagnetic transition of the Tb moments and it was accounted for by the change of the spiral plane of Mn moments from the bc plane to the ab plane.[13] Accordingly, the polarization at high fields is parallel to the a axis ($\mathbf{P} \parallel \mathbf{a}$). This type of ferroelectric phase is the one observed in compounds where the commensurate A-type magnetic ordering is preserved such as $GdMnO_3$.[14] For this compound, $\mathbf{P} \parallel \mathbf{a}$ only occurs when the magnetic field is applied along the b axis and it is clearly coupled to the metamagnetic transition of the Gd sublattice. This different behavior may arise from either the small anisotropy of Gd^{3+} cations or to structural differences as, e.g., the Mn-O-Mn bond angle. The value of this angle, which is higher in $GdMnO_3$, is related to the competition between superexchange magnetic interactions between nearest neighbors (NNs) and next-nearest neighbors (NNNs).[15] A strong competition stabilizes sinusoidal or ellipsoidal arrangements of the Mn moments.[15,16]

The importance of $J_{Mn\text{-}Tb}$ has been tested by the substitution of Mn with a nonmagnetic cation.[17–19] This substitution is detrimental to the Mn magnetic ordering that disappears for $x \sim 0.3$ well above the percolation limit for a metal with octahedral coordination. However, small substitutions have little effect on the magnetoelectric properties of the Mn sublattice but strongly affect the magnetic ordering of Tb moments indicating that such an ordering comes from the competition between $J_{Mn\text{-}Tb}$ and the direct coupling between Tb moments, $J_{Tb\text{-}Tb}$.[17]

In order to elucidate the effects of Mn dilution on the properties of $TbMnO_3$, we report here results obtained for the partial replacement of Mn^{3+} by Al^{3+}. This substitution is isovalent but the 17% difference in ionic size of Mn^{3+} and Al^{3+} (the ionic radii are 0.535 and 0.645 Å for Al^{3+} and Mn^{3+}, respectively)[20] may lead to a local disturbance of the lattice around the Al^{3+} ions to relax the strain produced by a

size mismatch. We studied the structural and magnetoelectric properties of both polycrystalline and single crystals of $TbMn_{1-x}Al_xO_3$ ($x = 0.05$ and 0.1). In addition, to probe the nature of the metamagnetic transitions, we report magnetic structures in a single crystal under an external magnetic field applied along the *b* axis.

II. EXPERIMENT

All the samples have been synthesized by a solid-state chemistry reaction. Stoichiometric amounts of Tb_4O_7, $MnCO_3$, and Al_2O_3 were mixed and heated at 1000 °C for 12 h in air. The resulting powders were pressed into pellets and sintered at 1200 °C for 24 h also in air. The last steps consisted of repressing and sintering the pellets at 1400 °C for 2 days in argon flow. X-ray powder diffraction patterns agree with a perovskite single phase. Attempts to prepare samples with $x \geqslant 0.2$ yielded a significant amount of secondary phases such as $Tb_4Al_2O_9$.[21] Single crystals of $TbMn_{1-x}Al_xO_3$ ($x =$ 0, 0.05, and 0.1) were grown by the floating method using a homemade furnace with two semielliptical mirrors.[22] The growth was carried out in Ar atmosphere. The feed and seed rods were rotating in opposite directions at ± 20 rpm and the growth speed was 6 mm/h. The chemical composition of both rods and boules was tested using a wavelength dispersive x-ray fluorescence spectrometer (Advant'XP + from Thermo-ARL) and the Tb:Mn:Al ratio agreed with the expected stoichiometry in all cases. Pieces of the boules were crushed into powder and the corresponding x-ray patterns showed a perovskite single phase.

X-ray diffraction patterns have been collected using a Rigaku D/max-B diffractometer with a copper rotating anode and a graphite monochromator in order to select the Cu K_α wavelength ($\lambda = 1.5418$ Å). The patterns were collected in a range $18^\circ \leqslant 2\theta \leqslant 130^\circ$ with a step $\Delta\theta = 0.03^\circ$, at room temperature. The integration time was 5 s/step. Neutron diffraction measurements were carried out at the Institut Laue-Langevin (ILL) in Grenoble (France) using two instruments. A powder specimen of $TbMn_{0.9}Al_{0.1}O_3$ was measured on the high-flux powder diffractometer D1B between 40 and 2 K in an angular range $10^\circ \leqslant 2\theta \leqslant 90^\circ$ with $\Delta\theta = 0.2^\circ$, using a wavelength of 2.52 Å. Measurements on a $TbMn_{0.9}Al_{0.1}O_3$ single crystal were performed on the single-crystal CRG-D15 diffractometer. The instrument, working at a wavelength of 1.173 Å, was used in the four-circle configuration, provided with a closed-cycle cryostat, for the measurements without applied magnetic field. The lifting-arm normal-beam configuration of the instrument, provided with an Oxford Instruments cryomagnet, was used for the study under applied magnetic field parallel to the *b* axis. The measurements were made under zero-field-cooled conditions. The software package program used for structural refinement was FULLPROF (Ref. 23) for both x-ray and neutron diffraction measurements.

The temperature dependence of the dc magnetization and ac magnetic susceptibility was measured in a commercial Quantum Design SQUID magnetometer from 2 K up to 295 K. Magnetic hysteresis loops were obtained at selected temperatures between −90 and 90 kOe using a commercial Quantum Design Physical Property Measurement System (PPMS). Heat capacity was also measured in the commercial PPMS using a relaxation technique. The temperature range was between 2 and 60 K with an external magnetic field up to 50 kOe. Electrical measurements were carried out on disk-shaped pellets with silver paste electrodes painted onto it. The complex impedance was measured between 100 Hz and 10 MHz with an impedance analyzer from Wayne Kerr Electronics (model 6500B). The measurements were performed in helium atmosphere from 4.2 K up to room temperature.

III. RESULTS

A. Room temperature crystal structure

The refinement of the x-ray diffraction pattern was used to test the quality of the samples and to obtain cell parameters with high precision. The results are summarized in Table I and compared to the parent $TbMnO_3$ compound.[6] The three compounds are isostructural adopting the orthorhombic cell of a perovskite (*Pbnm* space group). The absence of spurious diffraction peaks concurs with a perfect solid solution between Mn^{3+} and Al^{3+} cations in this concentration range.

The most noticeable effect produced by the substitution of Mn with Al is a decrease in the unit cell volume. This decrease is almost linear in this concentration range with a change of $\Delta V = -22.5$ Å$^3/x$. Such a result is expected because of the size difference between Mn^{3+} and Al^{3+} cations.[20] The contraction is mainly produced by the *b* axis shrinking ($\Delta b = -0.48$ Å$/x$) A small reduction is also observed in the *a* axis ($\Delta a = -0.09$ Å$/x$) while the *c* axis remains practically unchanged in the composition range studied. Accordingly, the orthorhombic distortion is reduced in the *ab* plane and this effect must be ascribed to the partial replacement of strongly distorted MnO_6 octahedra (Jahn-Teller-like) by the regular AlO_6 ones.[24]

B. Macroscopic properties

The occurrence of phase transitions was tested in the three compositions by measurements of the heat capacity. The temperature variations of specific heat are shown in Fig. 1. $TbMnO_3$ exhibits the three anomalies reported previously.[1] The two λ anomalies observed at $T_{N1} = 41.2$ K and $T_f = 26.1$ K are attributed to the magnetic ordering of Mn^{3+} moments and the ferroelectric transition, respectively. A big peak observed at $T_{N2} = 6.5$ K is ascribed to the magnetic ordering of Tb^{3+} moments. The partial replacement of Mn by Al affects the three transitions differently. $TbMn_{0.95}Al_{0.05}O_3$ also shows the three anomalies in the C_p/T curve. T_{N1} and T_f

TABLE I. Lattice parameters obtained from x-ray powder diffraction refinements at room temperature for $TbMn_{1-x}Al_xO_3$ ($x = 0.05$ and 0.1).

	$x = 0$*[a]	$x = 0.05$	$x = 0.1$
a (Å)	5.3019 (1)	5.29672(6)	5.29276 (3)
b (Å)	5.8557 (1)	5.83695(6)	5.80703 (3)
c (Å)	7.4009 (1)	7.39971(8)	7.40257 (4)
Volume (Å^3)	229.77	228.77	227.52

[a]Data taken from Ref. 6.

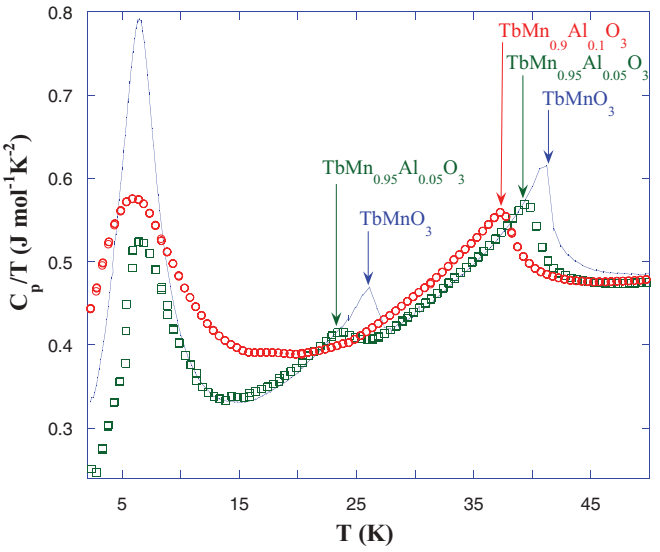

FIG. 1. (Color online) Temperature dependence of specific heat divided by temperature for $TbMnO_3$ (line), $TbMn_{0.95}Al_{0.05}O_3$ (squares), and $TbMn_{0.9}Al_{0.1}O_3$ (circles).

are shifted to lower temperatures appearing at 39.6 and 23.8 K, respectively. The former transition preserves the λ shape while the latter becomes more rounded and less intense. The peak at T_{N2} remains at the same temperature but its intensity (and the associated entropy content) is strongly reduced. In the $TbMn_{0.9}Al_{0.1}O_3$ sample only two anomalies are seen, the long-range magnetic ordering of Mn moments at $T_{N1} = 37.2$ K and a broad peak at 6 K, reminiscent of the anomaly associated to the ordering of Tb moments but with a shape that resembles a Schottky anomaly. There is no sign of anomaly corresponding to the ferroelectric transition but the background below 20 K is anomalously high in comparison to the other two samples.

The anisotropy present in these compounds is very clear in the magnetic properties. Figure 2(a) compares the magnetic hysteresis loops at 5 K for $TbMnO_3$ and $TbMn_{0.9}Al_{0.1}O_3$ along the three crystallographic axes. Overall, the two samples exhibit similar loops indicating that the isothermal magnetic curve at low temperature is mainly controlled by the magnetic properties of the Tb moments in this range of magnetic field ($H \leqslant 90$ kOe). The c axis is the hardest among the three main directions in the orthorhombic cell. The magnetization seems to increase linearly with the field although magnetic loops and spontaneous magnetization are clearly distinguished in both samples, in addition with a tiny magnetic transition around 50 kOe. Similar transitions have been previously reported for this geometry.[12] The other two principal directions show metamagnetic transitions and the magnetization does not achieve a complete magnetic saturation in our experimental range. For **H** ∥ **a**, both samples reach the maximum magnetization value at 90 kOe: 6.75 and 6.55 $\mu_B/f.u.$ (formula unit) for $x = 0$ and $x = 0.1$ respectively. They show a single metamagnetic transition at 17.5 ($x = 0$) and 16 kOe ($x = 0.1$). The critical fields are deduced from the inflection point in the magnetization curve [maximum in dM/dH curve shown in Fig. 2(b)].

For **H** ∥ **b**, two metamagnetic transitions are observed in the $TbMnO_3$ sample at 10 and 47 kOe in agreement with the results reported previously.[1,12] In this geometry, we have found

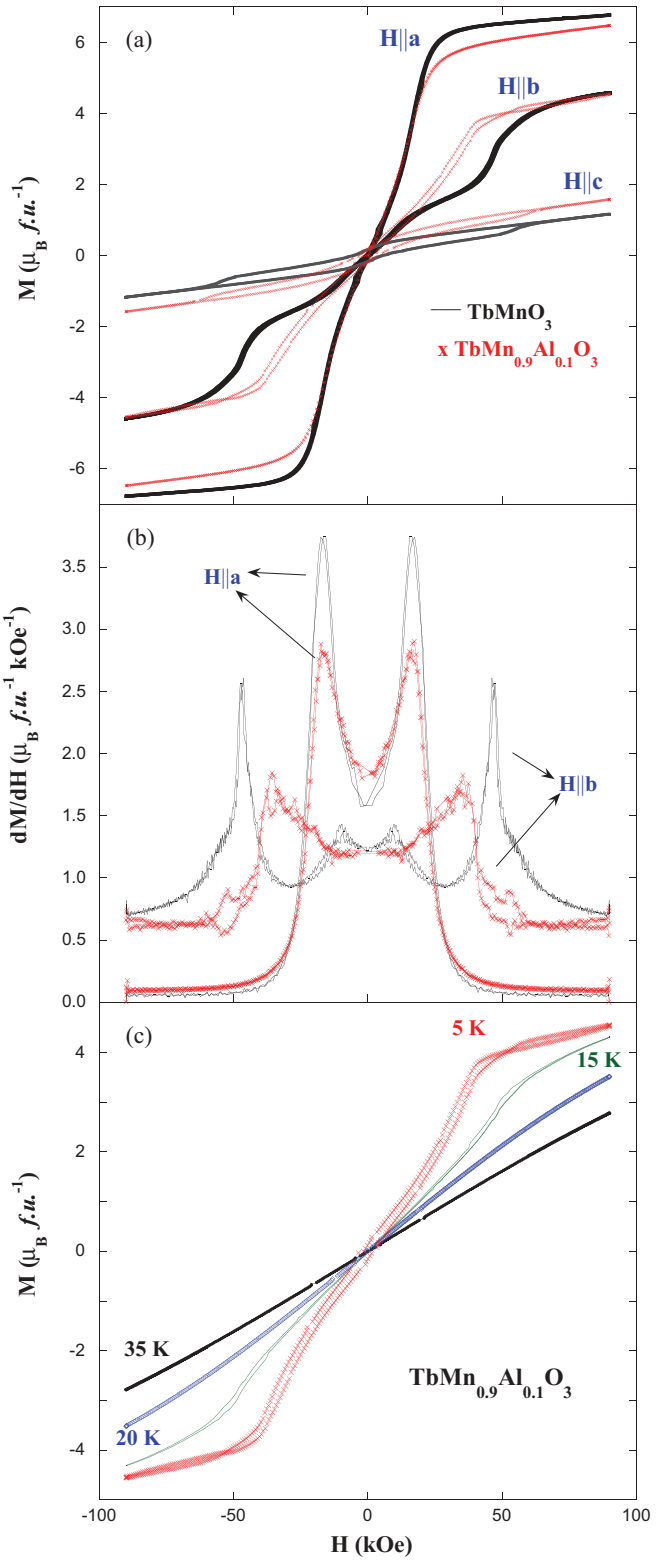

FIG. 2. (Color online) (a) Hysteresis loops of $TbMnO_3$ and $TbMn_{0.9}Al_{0.1}O_3$ at 5 K for the geometries indicated in the plot. (b) Derivative of magnetization with respect to H vs H. (c) Isothermal magnetization at selected temperatures for $TbMn_{0.9}Al_{0.1}O_3$.

the main differences between both samples. The two-step metamagnetic transition is smoothed for $TbMn_{0.9}Al_{0.1}O_3$ and there is no plateau centered at ∼30 kOe but a monotonic

increase in the magnetization with increasing H. This is also observed in the derivative plot in Fig. 2(b) where an asymmetric single peak is seen at ∼35 kOe. For this configuration, the magnetization of both samples reaches a value of 4.6 $\mu_B/f.u.$ at 90 kOe. The differences observed between **H** ∥ **a** and **H** ∥ **b** configurations can be understood on the basis of the magnetic ordering of Tb moments under an external field in a perovskite structure. Due to a strong Ising anisotropy, the Tb moments are usually ordered in noncollinear arrangements in the ab plane.[25] Following the representation analysis of Bertaut,[26] the high-field ordering of Tb moments would follow presumably the F_xC_y and C_xF_y symmetries for **H** ∥ **a** and **H** ∥ **b**, respectively, as was observed for $TbAlO_3$.[27] Depending on the ground-state ordering of Tb moments (**H** = 0) and the angle formed between the rare earth moments and the crystallographic axes (e.g., canting angle α respect to the x axis), one-step and two-step spin-flop transitions are observed at different directions in the ab plane.[27,28] It is noteworthy that the C_xF_y symmetry (**H**∥**b**) has been experimentally confirmed in the present work for $TbMn_{0.9}Al_{0.1}O_3$ (see neutron section later on). Assuming that the canting angle does not change with the strength of the magnetic field, we can deduce the magnetic components (m_x, m_y) of the Tb moments from the experimental magnetization values at 90 kOe [Fig. 2(a)] in **H** ∥ **a** and **H** ∥ **b** geometries and hence, $\tan\alpha = m_y/m_x$. The calculated values of these moments are 8.16 and 8.0 μ_B for $TbMnO_3$ and $TbMn_{0.9}Al_{0.1}O_3$. These values are smaller than the theoretical one (9 μ_B) but agree very well with the value experimentally found in related perovskites such as $TbAlO_3$ or $TbCoO_3$.[25] The angle formed between the moments and the a axis lies between 34° and 35°, also in good agreement with related perovskites.[25] Finally, the metamagnetic transition is still seen at 15 K for **H** ∥ **b** in the $TbMn_{0.9}Al_{0.1}O_3$ sample [see Fig. 2(c)] while the linear behavior at 35 K reveals a conventional paramagnetic contribution.

The temperature dependence of the magnetization for $TbMnO_3$ and $TbMn_{0.9}Al_{0.1}O_3$ along the principal axes is shown in Fig. 3. The results depend on the crystal orientation. For **H** ∥ **a** and **H** ∥ **b**, the magnetization decays with increasing the temperature for both samples. The temperature variation of the inverse of the susceptibility is linear in a wide temperature range (not shown here) as expected for paramagnetic materials obeying the Curie law. Only **H** ∥ **a** shows a clear peak attributed to the Tb magnetic ordering which is shifted to lower temperature for the Al-doped sample. The results are completely different for **H** ∥ **c**. The samples show the smallest value of magnetization in this geometry and several anomalies are observed in the curves [see Fig. 3(b)]. Three anomalies are observed below 50 K for $TbMnO_3$. The corresponding temperatures agree with the ones observed in the C_p/T measurements so they can be assigned to T_{N1}, T_f, and T_{N2}. $TbMn_{0.9}Al_{0.1}O_3$ shows only two anomalies (T_{N1} and T_{N2}) so this result also supports the lack of a ferroelectric transition for this sample. In addition, both samples exhibit a broad and rounded anomaly centered above 100 K [see inset of Fig. 3(b)]. This behavior has been observed in other Tb-based perovskites in this geometry,[29] including films of $TbMnO_3$.[30] Therefore, the temperature dependence of magnetic susceptibility for these compounds does not follow a simple Curie-Weiss law for **H** ∥ **c** since the interaction of Tb^{3+} with a crystal field

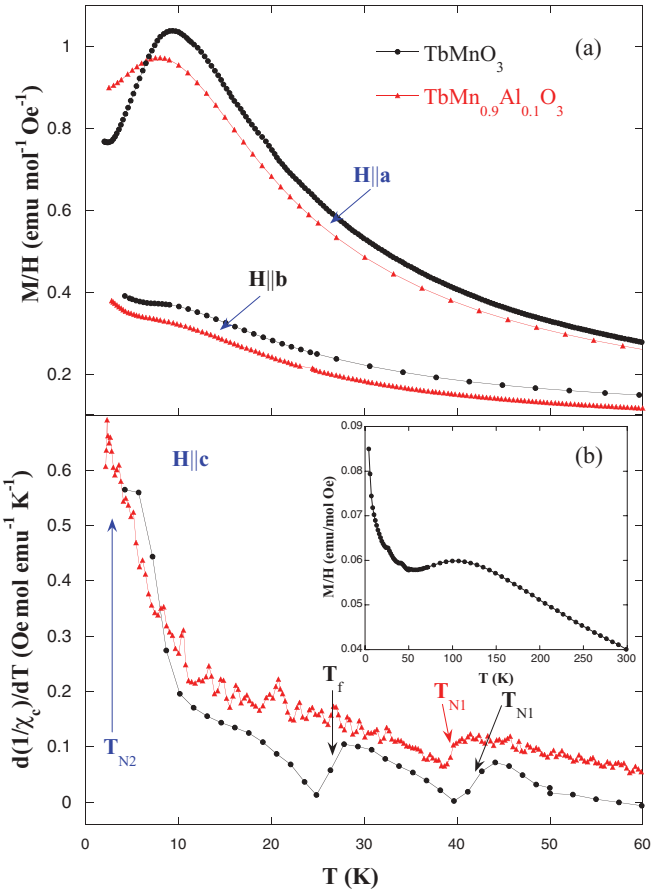

FIG. 3. (Color online) Magnetization taken at 5 kOe vs temperature for $TbMn_{1-x}Al_xO_3$ samples ($x = 0$ and 0.1). (a) **H** ∥ **a** and **H** ∥ **b**. (b) Derivative of inverse of magnetic susceptibility with respect to T vs temperature with **H** ∥ **c**. Inset: Magnetization of $TbMnO_3$ vs temperature for **H** ∥ **c**.

having Cs symmetry leads to an anisotropy in the magnetic properties.[27,29,31] The magnetic susceptibility in $TbAlO_3$ with **H** ∥ **c** was explained in terms of a significant contribution from excited states located in the $^7F_6$ manifold, which become thermally populated as the temperature is increased.[29] A similar feature is expected for $TbMnO_3$ and the mixing of excited states with the ground state associated with the Van Vleck mechanism leads to the nonlinear dependence of magnetization on temperature observed in the inset of Fig. 3(b).

The dielectric properties were also probed in these compounds. Figure 4(a) compares the temperature dependence of the real dielectric constant (ε') at low temperature for the three compositions. The measurements were performed on polycrystalline pellets. $TbMnO_3$ shows a sharp peak at T_f = 28 K which agrees with the reported ferroelectric transition for this sample.[1] $TbMn_{0.95}Al_{0.05}O_3$ exhibits a similar behavior with a peak at 24 K, in agreement with the anomalies observed in both C_p/T (T) and M (T) curves (see Figs. 1 and 3). The shape of the peak concurs with the strong anomaly observed in $TbMnO_3$ single crystals with electric field parallel to the c axis (**E** ∥ **c**).[1,17] Therefore, $TbMn_{0.95}Al_{0.05}O_3$ seems to undergo a ferroelectric transition, similarly to the parent compound, with

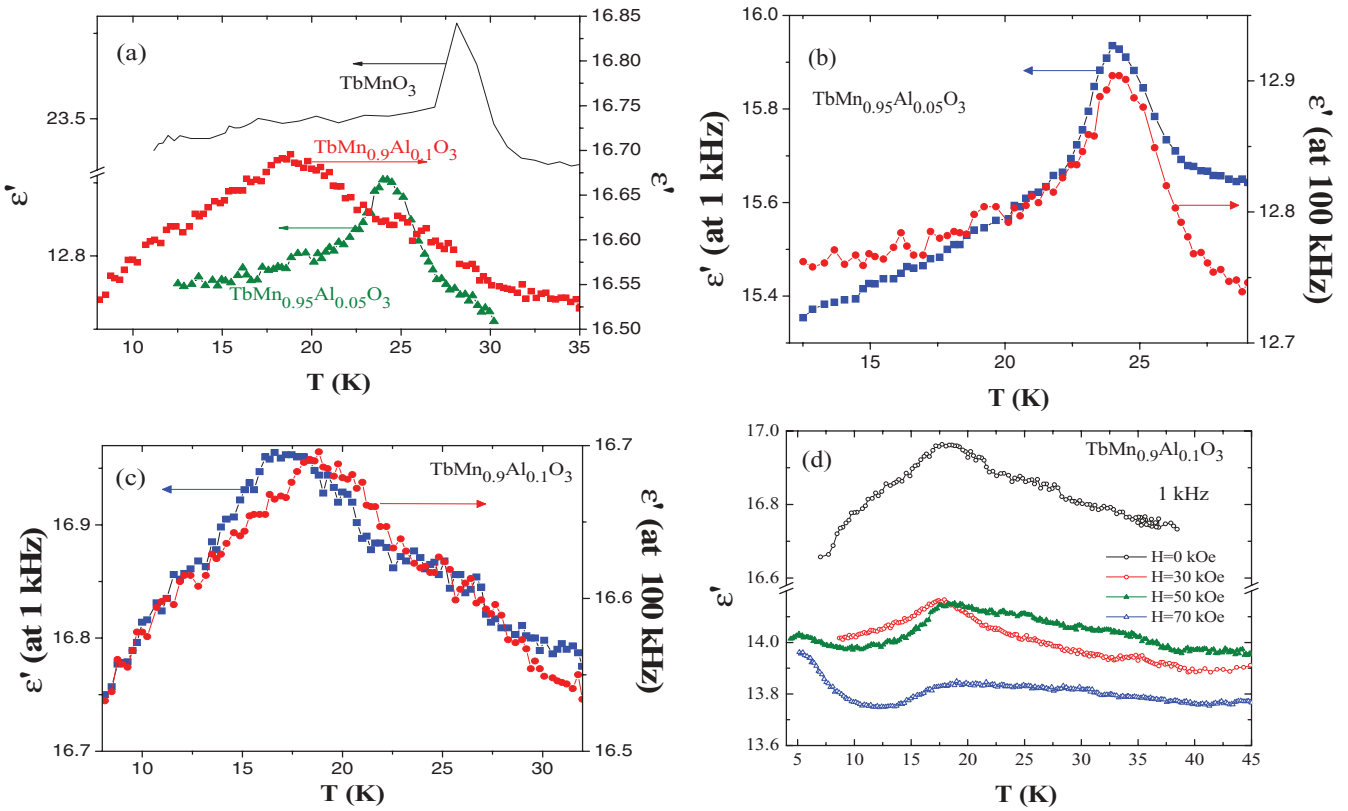

FIG. 4. (Color online) (a) Real dielectric constant at 100 KHz for $TbMn_{1-x}Al_xO_3$ samples ($x = 0$, 0.05, and 0.1). Comparison of real dielectric constant at 1 and 100 KHz for (b) $TbMn_{0.95}Al_{0.05}O_3$ and (c) $TbMn_{0.9}Al_{0.1}O_3$. (d) Comparison of real dielectric constant at 100 KHz of $TbMn_{0.9}Al_{0.1}O_3$ under different magnetic fields.

presumably $\mathbf{P} \parallel \mathbf{c}$. However, $TbMn_{0.9}Al_{0.1}O_3$ shows a different anomaly in the temperature variation of ε'. A broad peak is observed at $T_p \sim 18$ K contrary to the sharp peak of the other two compounds. The measurements at different frequencies reveal more differences. Figures 4(b) and 4(c) compare the results at 1 and 100 KHz for both samples. The peak of the $TbMn_{0.95}Al_{0.05}O_3$ samples does not change with the frequency. However, the dielectric anomaly of $TbMn_{0.9}Al_{0.1}O_3$ becomes broader and shifts toward higher temperature with increasing frequency, which resembles a relaxor behavior.

The influence of an external $\mathbf{H}$ on the ε' was also studied in $TbMn_{0.9}Al_{0.1}O_3$ and the results are displayed in Fig. 4(d). The broad peak disappears at $H > 30$ kOe and for $H = 70$ kOe, the temperature variation of ε' shows an abrupt decay at a similar temperature (~17 K). This resembles the behavior observed in both $TbMnO_3$ and $GdMnO_3$ for the geometry $\mathbf{E} \parallel \mathbf{a}$ and high $\mathbf{H}$. Both compounds develop polarization along the a axis ($\mathbf{P} \parallel \mathbf{a}$) above a critical field H_C. In the case of $TbMnO_3$, the appearance of this ferroelectric phase is coupled to a spin flop of the cycloid ordering of Mn moments from the bc plane to the ac plane. Consequently, the polarization direction changes from $\mathbf{P} \parallel \mathbf{c}$ (below H_C) to $\mathbf{P} \parallel \mathbf{a}$ (above H_C). In the case of $GdMnO_3$, the transition induced by H is from a conventional A-type magnetic structure ($P = 0$ below H_C) to a ferroelectric phase with $\mathbf{P} \parallel \mathbf{a}$ above H_C.[14] Bearing in mind these references, the changes in $\varepsilon'(H)$ observed in $TbMn_{0.9}Al_{0.1}O_3$ might be ascribed to a transition from a relaxor to a ferroelectric state.

C. Zero-field neutron diffraction measurements

The magnetic structure of the samples doped with Al was studied by neturon powder diffraction. Superstructure peaks arising from the ordering of Mn moments are clearly visible below ~39.5 and ~37 K for $TbMn_{0.95}Al_{0.05}O_3$ and $TbMn_{0.9}Al_{0.1}O_3$, respectively. Figure 5(a) compares the neutron powder patterns at 2 and 39 K for both samples. The magnetic reflections agree with an incommensurate ordering of the A type, as already found in $TbMnO_3$, with a propagation vector $\mathbf{k}_{Mn} = (0, q_{Mn}, 0)$ which varies with temperature. Figure 5(b) shows the temperature dependence of q_{Mn} obtained from the patterns. Overall, the behavior is similar to the one reported for $TbMnO_3$ but q_{Mn} decreases with increasing the Al content in the sample, approaching the commensurate value of 1/4. The value of q_{Mn} decreases with the temperature down to ~24 K, to a minimum value of ~0.27 and ~0.26 r.l.u. (reciprocal lattice units) for $TbMn_{0.95}Al_{0.05}O_3$ and $TbMn_{0.9}Al_{0.1}O_3$, respectively. Below 24 K, q_{Mn} remains practically constant within the experimental error. This behavior resembles a lock-in transition and it seems to be a general feature of this type of manganite, independently of the electric ground state (ferroelectric or not) as was suggested in the study of $Gd_{1-x}Tb_xMnO_3$ series.[32] The observation of the same feature in the evolution of q_{Mn} in $TbMn_{0.9}Al_{0.1}O_3$ possessing a relaxor behavior confirms the lack of correlation between ferroelectricity and the so-called lock-in transition of q_{Mn}. The pattern at 2 K also shows a broad peak centered around $2\theta \sim 22.5^\circ$ for $TbMn_{0.95}Al_{0.05}O_3$ that is attributed to a short-range

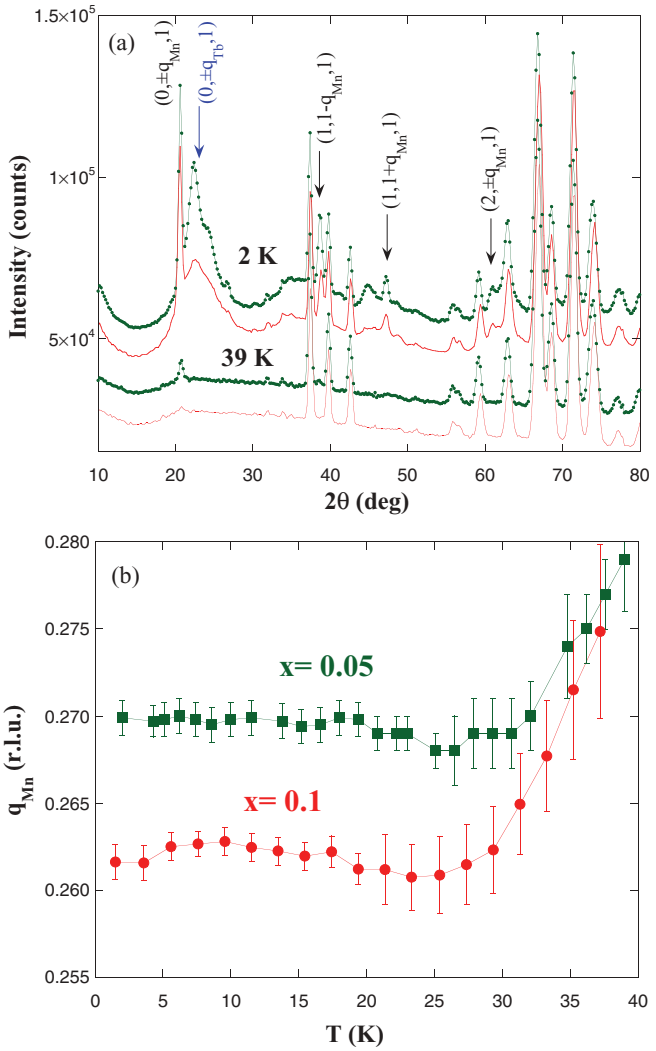

FIG. 5. (Color online) (a) Neutron powder diffraction at 2 and 39 K for $TbMn_{0.95}Al_{0.05}O_3$ (line + points) and $TbMn_{0.9}Al_{0.1}O_3$ (single line). The patterns have been shifted vertically for the sake of comparison. (b) Temperature dependence of the *b* component in the modulation vector for both samples.

ordering of Tb^{3+} moments as observed in related compounds. This ordering agrees with a wave vector $\mathbf{k}_{Tb} = (0, q_{Tb} \sim 0.43, 0)$ and the relationship $3q_{Tb}-q_{Mn} = 1.02$ (~ 1) is fulfilled in this compound indicating the coupling between both sublattices. This peak becomes very broad in $TbMn_{0.9}Al_{0.1}O_3$ revealing a decrease of the magnetic coherence length that may arise from the weakness of the coupling between Tb and Mn lattices.

In order to gain insight into the type of magnetic ordering of $TbMn_{0.9}Al_{0.1}O_3$, a neutron diffraction study on a single crystal was performed. Preliminary studies were carried out and the diffraction intensity along the (0, *k*, 1) and (0, *k*, 2) directions of reciprocal space at three selected temperatures was probed. The results are displayed in Figs. 6(a) and 6(b). At 20 K, we have found two types of magnetic reflections ascribed to the ordering of Mn moments. The most intense reflections correspond to the previously mentioned *A*-type reflections obeying the extinction conditions $h + k =$ odd and $l =$ even. Moreover, we detect weak reflections of *G* type with the extinction conditions $h + k =$ even, $l =$ even. The calculated q_{Mn} for the single crystal is 0.255, and the slight change with respect to the powder diffraction characterization may be due to either differences in the experimental setup or slight changes in the composition between single crystal and powder specimen.

At 2 K, we observe an additional magnetic scattering that is ascribed to the Tb^{3+} moments. Figure 6(b) shows the appearance of weak peaks in the reciprocal space associated to *F*-type (extinction conditions: $h + k =$ odd, $l =$ odd) and *C*-type ($h + k =$ even, $l =$ odd) magnetic contributions. These magnetic peaks are, as well, incommensurate with $\mathbf{k}_{Tb} = (0, q_{Tb} \sim 0.35, 0)$. q_{Tb} is strongly reduced compared to the parent compound and the relationship $3q_{Tb}-q_{Mn} \approx 1$ fulfilled in $TbMnO_3$ is no longer valid for $TbMn_{0.9}Al_{0.1}O_3$. This result reveals that Al substitution is very detrimental for the magnetic correlation between Mn and Tb sublattices. An anomalous increase of the background can be observed in Fig 6(a) at 2 K which should be linked to *A*-type reflections arising from the magnetic contribution of Tb^{3+} moments of very short range which partly overlap the magnetic peaks from Mn^{3+} moments.

The temperature evolution of representative magnetic reflections for the Mn^{3+} ordering was monitored. Figure 6(c) shows the magnetic onset of Mn^{3+} ordering at $T_{N1} \sim 37$ K that is visible for both type of magnetic reflections (*A* and *G*). Figure 6(d) shows the temperature dependence of these kinds of magnetic reflections at lower temperature. A sudden decrease in the integrated intensity is observed at 8 K correlated to the onset of the Tb^{3+} magnetic ordering. Similar features have been reported in related compounds[8,33] but this result must be taken with care as the determination of the peak intensities is blurred by the anomalous background increase related to the observed diffuse scattering in Fig. 6(a).

Taking into account the previous results, the crystal and magnetic structures were determined at 20 K on a single crystal with cylindrical shape (diameter of $\sim$3 mm and length of $\sim$2.5 mm). Measurements were taken of 180 nuclear reflections, and the crystal structure can be refined in the *Pbnm* space group using isotropic temperature factors. The structural results are summarized and compared to those of $TbMnO_3$ in Table II. Figure 7(a) presents the comparison between the observed and calculated intensities. The reliability factor based on integrated intensity is $R_I = 0.030$ with $\chi^2 = 1.2$. Despite the structural similarities between the two compounds, there are significant changes in the local environment of Mn (and Al). Firstly, the average Jahn-Teller distortion is reduced in the $Mn(Al)O_6$ octahedron. This result is likely due to the dilution of active Jahn-Teller cations (Mn^{3+}) with closed shells cations (Al^{3+}). Secondly, the substitution with Al increases the *M*-O-*M* bond angle reaching values very close to those observed in a $GdMnO_3$ sample as inferred from the phase diagram reported in Ref. 14. We used 128 magnetic reflections (satellites $\pm q_{Mn}$) to determine the magnetic structure at 20 K. Representation symmetry analysis using the BASIREPS program[34] was used to find the irreducible representations (*Irreps*) contained in Γ to describe magnetic structures. The possibilities are collected in Table III. The ordering of Mn^{3+} moments can be accounted for by the single *Irrep* Γ_3. The refined magnetic components per Mn are $m_x = -0.39(2)$

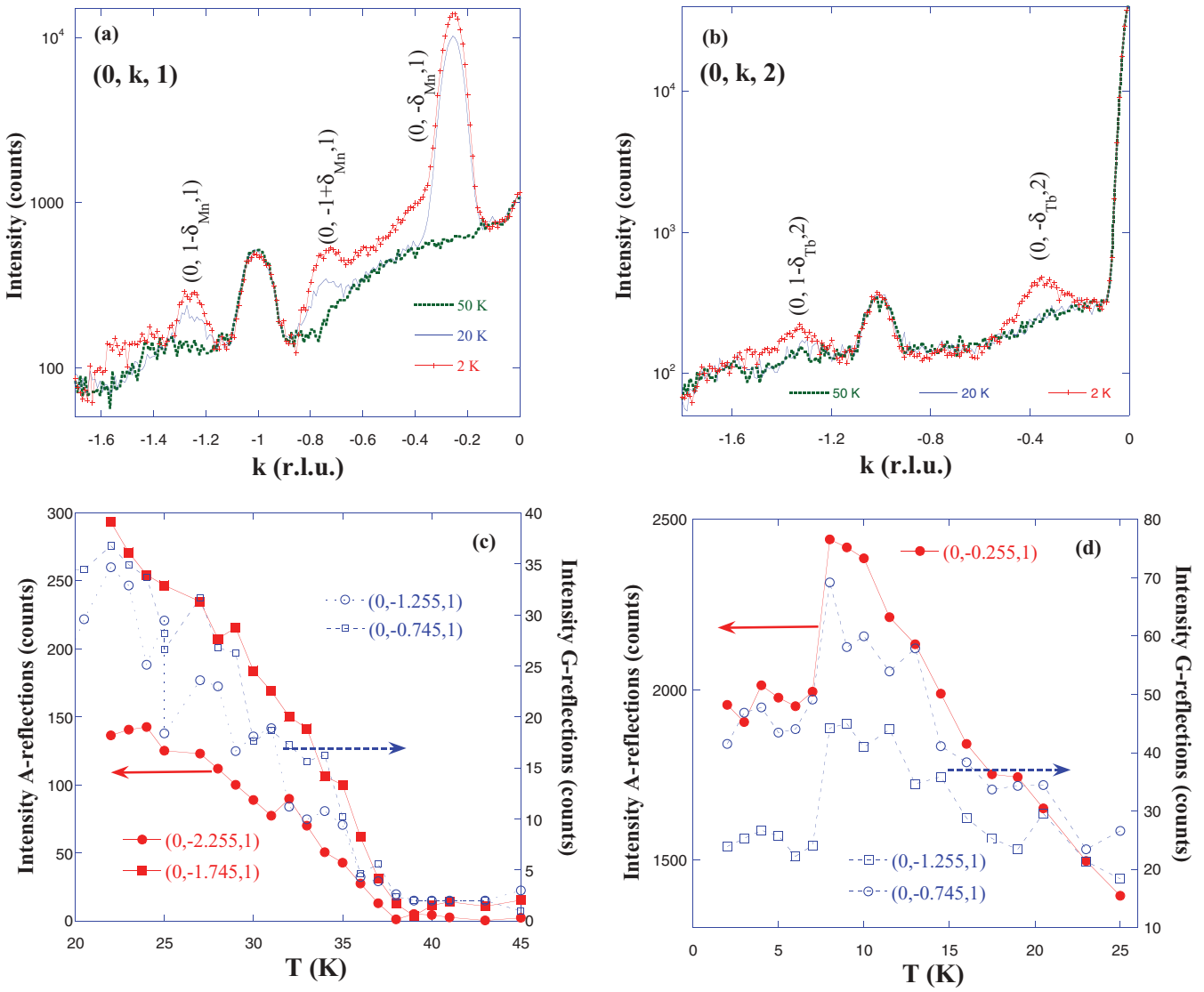

FIG. 6. (Color online) Diffraction intensity along (a) the $(0, k, 1)$ and (b) the $(0, k, 2)$ directions. Temperature evolution of selected diffraction peaks around (c) the long-range ordering of Mn^{3+} moments and (d) the magnetic ordering of Tb^{3+} moments.

and $m_y = 2.99(1)$. The main y component is sinusoidally modulated along the b axis following an A-type ordering whereas the x component can be considered as a small canting following a G-type ordering. Some very weak ferromagnetic reflections were also detected so a ferromagnetic component along the c axis, compatible with *Irrep* Γ_3 (see Table III), was also refined yielding a value of $m_z = 0.15(10)$. However, the origin of this component is unclear. The comparison between the observed and calculated intensities is displayed in Fig. 7(b).

D. Neutron diffraction under an external magnetic field

A cryomagnet was coupled to the diffractometer to study the effect of an external magnetic field on the magnetic structure but the experimental setup limits the available range of reflections. We started our study at 15 K, below the peak observed in the ε' measurements [see Fig. 4(a)]. At zero field, no change is seen. Applying a magnetic field ($\mathbf{H} \parallel \mathbf{b}$), several changes are observed. The scattering associated to the incommensurate Tb^{3+} ordering vanishes while the satellite reflections associated to the Mn^{3+} ordering remains practically unchanged. In addition we observe an intensity increase in some nuclear reflections indicating that magnetic field induces a long-range ordering of Tb^{3+} moments, which is commensurate with a propagation vector $\mathbf{k} = (0, 0, 0)$. This kind of metamagnetic transition has also been observed in macroscopic measurements (see Fig. 2). Representation analysis was again employed to determine the Tb^{3+} magnetic ordering. The possibilities are summarized in Table IV. Eighty-nine nuclear reflections were used to refine the structural parameters and the Tb magnetic moments. Two magnetic fields were probed (30 and 60 kOe) and the results were similar for both. The Tb magnetic structure can be described by the single *Irrep* Γ_7' (prime is used to differentiate it from the *Irrep*s of Mn ordering) which in Bertaut's notation corresponds to a $C_x F_y$ type of magnetic ordering. The refined components are $\mathbf{m}_{Tb} = [1.66(36), 1.45(11), 0]$ and $\mathbf{m}_{Tb} = [3.78(17), 2.75(7), 0]$ for 30 and 60 kOe, respectively. This result confirms the noncollinear

TABLE II. Comparison of structural parameters (unit cell, fractional coordinates, bond lengths, and bond angles) and reliability factors for the neutron diffraction refinements of a powder specimen of $TbMnO_3$ (Ref. 6) and a single crystal of $TbMn_{0.9}Al_{0.1}O_3$. *M* refers to Mn and Al.

	$x = 0$[a]	$x = 0.1$
a (Å)	5.3019 (1)	5.2821(1)
b (Å)	5.8557 (1)	5.7504(1)
c (Å)	7.4009 (1)	7.4028(2)
Tb: *x*	0.9836(1)	0.9847(3)
y	0.0810(2)	0.0767(3)
B (Å^2)	0.84(1)	0.07(6)
M: *B* (Å^2)	0.75(2)	0.11(8)
O1: *x*	0.1083(8)	0.1046(3)
y	0.4694(8)	0.4683(3)
B (Å^2)	0.94(7)	0.20(5)
O2: *x*	0.7033(2)	0.7047(2)
y	0.3242(3)	0.3226(2)
z	0.0530(2)	0.0501(1)
B (Å^2)	0.94(7)	0.23(4)
M-O1	1.946(1)	1.9400(5)
M-O2	2.243 (4)	2.1790(11)
M-O2	1.889 (4)	1.9004(11)
⟨*M*-O(1)-*M*⟩	144.0 (1)	145.10(2)
⟨*M*-O(2)-*M*⟩	145.7 (1)	146.20(4)
R_{Bragg} (%)	4.2	3.05
		$\chi^2 = 1.25$

[a]Reference 6.

arrangement of Tb^{3+} moments under an external field. The strongest component is along the *a* axis, the softest magnetic axis among the three principal directions of the crystal. Most likely, the magnetic structure for $\mathbf{H} \parallel \mathbf{a}$ is F_xC_y (*Irrep* Γ_5' in Table IV). Finally, the magnetic components at 60 kOe yield a canting angle of 35.7° with respect to the *a* axis for the Tb^{3+} moments, in good agreement with results obtained from isothermal magnetization (see Fig. 2).

The magnetic structure of Mn^{3+} moments was obtained from 59 magnetic reflections, and the results are similar to the ones obtained previously at 20 K. The refined components were $\mathbf{m}_{Mn}$ = [–0.52(3), 3.37(1), 0] and $\mathbf{m}_{Mn}$ = [–0.60(3), 3.57(2), 0] for H = 30 and 60 kOe, respectively. The Mn preserves the sinusoidal magnetic ordering up to 60 kOe at 15 K, and the only field-induced change is a slight increase of the moment magnitude as H increases.

The strong diffuse magnetic scattering observed at 2 K coming from the short-range ordering of Tb^{3+} moments did not allow accurate refinements at zero field. This scattering is suppressed by applying a magnetic field due to the metamagnetic transition of Tb^{3+} moments. Therefore, we successfully refined the nuclear reflections at 30 kOe. The crystal cell parameters are similar to the ones at 20 K (see Table II) and the Tb^{3+} moments exhibit again the noncollinear arrangement of C_xF_y type. The refined moment is $\mathbf{m}_{Tb}$ = [2.57(2), 1.69 (4), 0] μ_B which yields a canting angle of 33.3° relative to the *a* axis. The Mn magnetic ordering can be determined from satellite reflections. The measurements were carried out at H = 30 and 60 kOe. At 30 kOe, diffuse scattering is still significant in many satellite reflections (see Fig. 8)

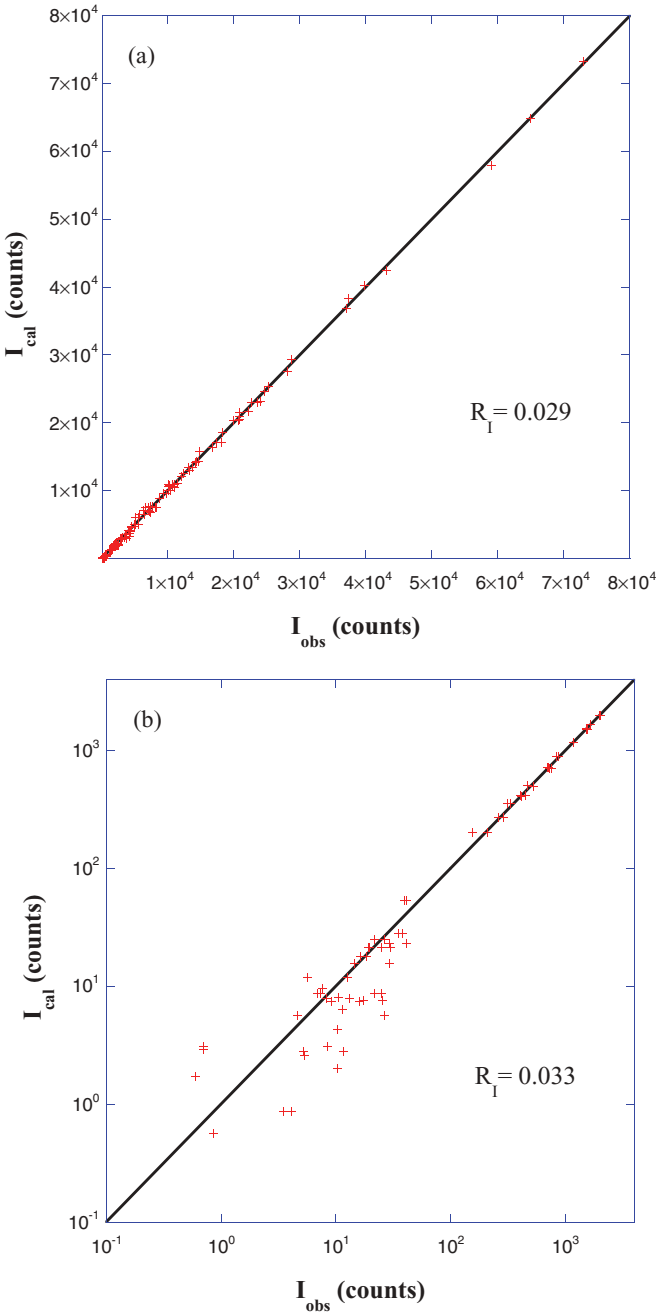

FIG. 7. (Color online) Comparison between observed and calculated intensities of single-crystal neutron diffraction measurement for (a) nuclear and (b) magnetic reflections of $TbMn_{0.9}Al_{0.1}O_3$ at 20 K.

making it very difficult to extract a reliable magnetic structure. This scattering is completely suppressed at 60 kOe, so this measurement was used to determine the magnetic structure of Mn^{3+} moments at high field. The refinement with a sinusoidal model (single *Irrep* Γ_3) yielded poor results with $R_I \sim$ 11.2 and $\chi^2 \sim 6$. Following Ref. 7, we have a tried linear combination of two *Irrep*s and the best results were obtained for the $\Gamma_1 \oplus \Gamma_3$ combination yielding fits with $R_I = 3.6$ and $\chi^2 = 1.2$. The phase shift between both components is $\pi/2$, i.e., the maximum in the *a* component concurs with the minimum in the *b* component and vice versa. The refined components are $\mathbf{m}^1_{Mn}$ = [1.67(9), 0, 0] μ_B and $\mathbf{m}^3_{Mn}$ = [0,

TABLE III. Irreducible representation of the group Γ_k for the incommensurate structure with $\mathbf{k} = (0, q_{\mathrm{Mn}} = 0.255, 0)$, basis vectors for the atom (Mn, Al) located at the 4*b* Wyckoff position and magnetic type ordering following Bertaut's notation (Ref. 26); a_R (~ 0.696) is the real component of the complex phase a.

Γ_k	1	2_y	m_{xy}	m_{yz}	Mn (1) (1/2 0 0)	Mn (2) (0 1/2 1/2)	Mn (3) (1/2 0 1/2)	Mn (4) (0 1/2 0)	Ordering type
Γ_1	1	a	1	a	(1 0 0)	$(-a_R\ 0\ 0)$	$(-1\ 0\ 0)$	$(a_R\ 0\ 0)$	A_x
					(0 1 0)	$(0\ a_R\ 0)$	$(0\ -1\ 0)$	$(0\ -\ a_R\ 0)$	G_y
					(0 0 1)	$(0\ 0\ -\ a_R)$	(0 0 1)	$(0\ 0\ -\ a_R)$	C_z
Γ_2	1	a	-1	$-a$	(1 0 0)	$(-a_R\ 0\ 0)$	(1 0 0)	$(-a_R\ 0\ 0)$	C_x
					(0 1 0)	$(0\ a_R\ 0)$	(0 1 0)	$(0\ a_R\ 0)$	F_y
					(0 0 1)	$(0\ 0\ -\ a_R)$	$(0\ 0\ -1)$	$(0\ 0\ a_R)$	A_z
Γ_3	1	$-a$	1	$-a$	(1 0 0)	$(a_R\ 0\ 0)$	$(-1\ 0\ 0)$	$(-a_R\ 0\ 0)$	G_x
					(0 1 0)	$(0\ -\ a_R\ 0)$	$(0\ -1\ 0)$	$(0\ a_R\ 0)$	A_y
					(0 0 1)	$(0\ 0\ a_R)$	(0 0 1)	$(0\ 0\ a_R)$	F_z
Γ_4	1	$-a$	-1	a	(1 0 0)	$(a_R\ 0\ 0)$	(1 0 0)	$(a_R\ 0\ 0)$	F_x
					(0 1 0)	$(0\ -\ a_R\ 0)$	(0 1 0)	$(0\ -\ a_R\ 0)$	C_y
					(0 0 1)	$(0\ 0\ a_R)$	$(0\ 0\ -1)$	$(0\ 0\ -\ a_R)$	G_z

3.15(3), 0] μ_{B} (superscripts denote the corresponding *Irrep*). Therefore, the moments form an elliptical spiral in the *ab* plane propagating along the *b* direction, i.e., the *ab*-cycloid magnetic structure which has been found in related manganites with spontaneous $\mathbf{P} \parallel \mathbf{a}$.[13] These results support an electric phase transition from a relaxor behavior to a ferroelectric state ($\mathbf{P} \parallel \mathbf{a}$) driven by an external magnetic field in the $\mathbf{H} \parallel \mathbf{b}$ geometry.

In this measurement, very weak reflections of *G* type are still visible. There are two possibilities to account for these reflections: (i) a canting of the moments along the *z* direction following a *G*-type ordering, or (ii) the occurrence of phase segregation (the sinusoidal phase is not completely transformed to a cycloid structure at 60 kOe). The latter is less likely taking into account the good agreement found for the strongest *A*-type reflections. The first possibility implies the linear combination of three *Irrep*s, $\Gamma_1 \oplus \Gamma_3 \oplus \Gamma_4$ (see Table IV). The refinement of a G_z component in phase with the *y* component yielded a value of $\mathbf{m}_z = 0.49(17)$ in accordance with the weak contribution of this component to the magnetic structure.

IV. DISCUSSION AND CONCLUSIONS

The low substitution of Mn for Al affects significantly the magnetoelectric properties of $TbMnO_3$. First of all, it leads to the expected weakening of the superexchange Mn-O-Mn interaction due to the dilution of magnetic ions. This explains the gradual decrease of T_{N1} in the $TbMn_{1-x}Al_xO_3$ series with increasing x at a rate of -39 K x^{-1} (for $x \leqslant 0.1$ range). Similar results were obtained for dilution with other nonmagnetic trivalent cations such as Ga^{3+} or Sc^{3+}.[17–19] The Mn ordering remains incommensurate in the $TbMn_{1-x}Al_xO_3$ samples studied, with a sinusoidal modulation of the moment magnitude along the *b* axis. However, the wave-vector component is very close to the commensurate value of $q_{\mathrm{Mn}} \sim 1/4$ for $TbMn_{0.9}Al_{0.1}O_3$.

This type of substitution also strongly affects the ferroelectric ordering observed in $TbMnO_3$. For $TbMn_{0.95}Al_{0.05}O_3$, T_f decreases about 3 K as compared to $TbMnO_3$ while for $TbMn_{0.9}Al_{0.1}O_3$, the temperature variation of the dielectric constant does not present the typical anomaly of a ferroelectric ordering but a broad peak at $T_p \sim 18$ K whose position

TABLE IV. Irreducible representation of the group Γ_k for the magnetic structure with $\mathbf{k} = (0, 0, 0)$, basis vectors for the Tb atom located at the 4*c* Wyckoff position and magnetic type ordering following Bertaut's notation (Ref. 26).

Γ'_k	1	2_z	2_x	2_y	Tb (1) ($\sim 0 \sim 0\frac{1}{4}$)	Tb (2) ($\sim 0 \sim \frac{1}{2}\frac{3}{4}$)	Tb (3) ($\sim \frac{1}{2} \sim 0\frac{3}{4}$)	Tb (4) ($\sim \frac{1}{2} \sim \frac{1}{2}\frac{3}{4}$)	Order type
Γ'_1	1	1	1	1	(0 0 1)	(0 0 1)	$(0\ 0\ -1)$	$(0\ 0\ -1)$	C_z
Γ'_2	1	1	1	1	(1 0 0)	$(-1\ 0\ 0)$	(1 0 0)	$(-1\ 0\ 0)$	A_x
					(0 1 0)	$(0\ -1\ 0)$	$(0\ -1\ 0)$	(0 1 0)	G_y
Γ'_3	1	1	-1	-1	(0 0 1)	(0 0 1)	(0 0 1)	(0 0 1)	F_z
Γ'_4	1	1	-1	-1	(1 0 0)	$(-1\ 0\ 0)$	$(-1\ 0\ 0)$	(1 0 0)	G_x
					(0 1 0)	$(0\ -1\ 0)$	(0 1 0)	$(0\ -1\ 0)$	A_y
Γ'_5	1	-1	1	-1	(1 0 0)	(1 0 0)	(1 0 0)	(1 0 0)	F_x
					(0 1 0)	(0 1 0)	$(0\ -1\ 0)$	$(0\ -1\ 0)$	C_y
Γ'_6	1	-1	1	-1	(0 0 1)	$(0\ 0\ -1)$	$(0\ 0\ -1)$	(0 0 1)	G_z
Γ'_7	1	-1	-1	1	(1 0 0)	(1 0 0)	$(-1\ 0\ 0)$	$(-1\ 0\ 0)$	C_x
					(0 1 0)	(0 1 0)	(0 1 0)	(0 1 0)	F_y
Γ'_8	1	-1	-1	1	(0 0 1)	$(0\ 0\ -1)$	(0 0 1)	$(0\ 0\ -1)$	A_z

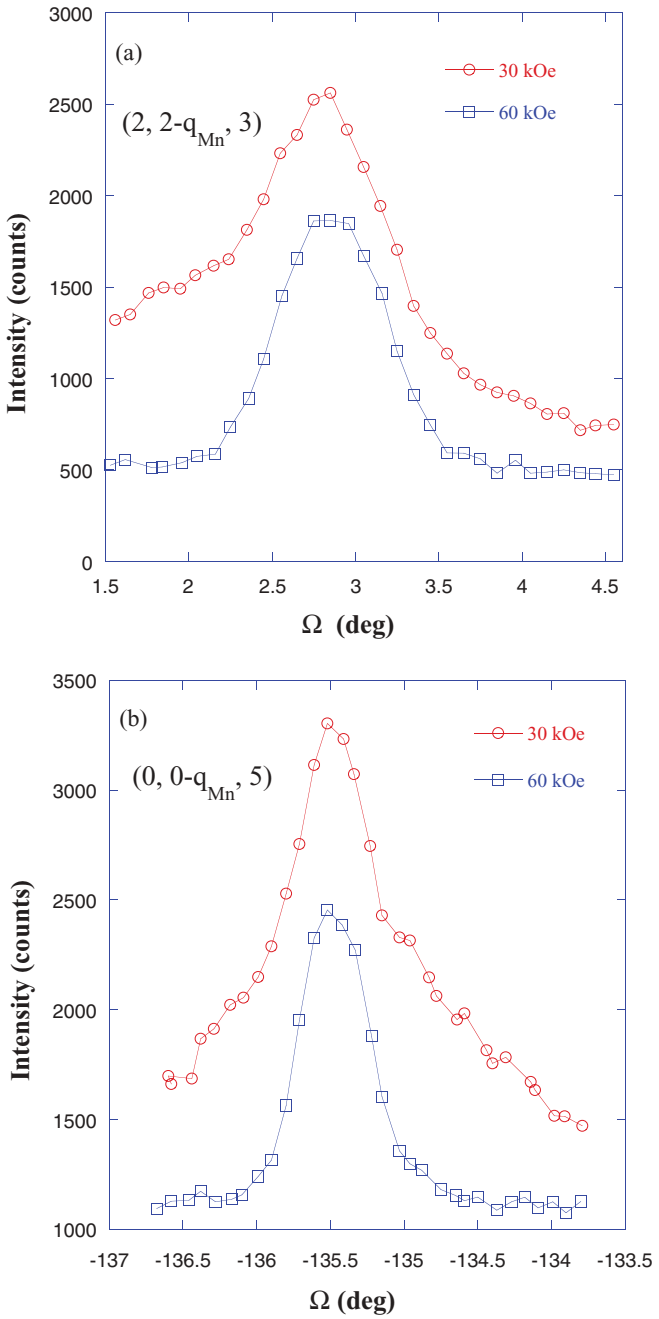

FIG. 8. (Color online) Rocking curves of selected diffraction peaks (a) (h, h-q_{Mn}, l) type and (b) (0, 0-q_{Mn}, l) type for $TbMn_{0.9}Al_{0.1}O_3$ at magnetic fields of 30 and 60 kOe.

depends on the frequency of the electric field in a manner similar to the behavior of a relaxor. In addition, measurements of C_p/T and magnetic susceptibility do not reveal a clear anomaly associated with the ferroelectric order for this composition. These measurements are consistent with the presence of nanoscale polar domains not leading to a long-range ferroelectric ordering. $TbMnO_3$ undergoes a Mn^{3+} spin reordering at T_f, in which a component along the z direction emerges giving rise to the so-called cycloid structure in the bc plane.[7] Therefore, FE and magnetic reordering are coupled in $TbMnO_3$. The lack of FE in $TbMn_{0.9}Al_{0.1}O_3$ is compatible with the stability of the sinusoidal ordering of Mn^{3+} moments (no magnetic rearrangement) below T_p as observed by neutron diffraction at 15 K.

The presence of a relaxor behavior at zero magnetic field, observed upon Al dilution, has not been found in the substitution of Ga for Mn.[17] This might be due to the small size of Al^{3+} which leads to a decrease of the unit cell volume. Hence, it is worth comparing the properties of $TbMnO_3$ under hydrostatic pressure. Recent studies have reported a pressure-induced change in the magnetic structure of $TbMnO_3$ which adopts an E-type structure above 3.6 GPa, similar to $HoMnO_3$ at ambient pressure.[35] This is not the case for the Al-doped samples studied in this work. This fact might be due either to an insufficient volume reduction by doping ("chemical pressure") or to the inhomogeneity of the Mn sublattice. The other significant structural effect produced by the substitution of Mn with Al is an increase of the M-O-M bond angle (M = Mn, Al) as deduced from neutron diffraction refinements (see Table II). This result can be understood phenomenologically using the Goldschmidt[36] tolerance factor defined in our case as t = Tb-O/($\sqrt{2}\times$ M-O), Tb-O and M-O being the bond lengths. An ideal cubic perovskite with M-O-M = 180° (maximum strength for NN magnetic interactions) is observed for $t = 1$. A decrease of t (smaller bond length in the numerator) leads to distorted structures and to a decrease of M-O-M bond angle. As Mn^{3+} is replaced by much smaller Al^{3+}, M-O decreases (decreasing the denominator) and thus t becomes larger which implies an increase in the M-O-M bond angle (see Table II). The increase of this angle may change the balance between NN and NNN interactions. In fact, the bond angle observed in $TbMn_{0.9}Al_{0.1}O_3$ is similar to that found in $GdMnO_3$ so it is noteworthy to compare the properties of both compounds. Contradictory results have been published for $GdMnO_3$. Some authors suggest the presence of spontaneous polarization $\mathbf{P} \parallel \mathbf{a}$ at zero field[14,37] while others indicate that $\mathbf{P} \parallel \mathbf{a}$ only appears when a magnetic field is applied along the b axis.[12] These discrepancies point to the strong effects brought by small changes in the stoichiometry of the samples. In fact, the study of $Tb_{1-x}Gd_xMnO_3$ compounds reveals a region in the phase diagram, close to $GdMnO_3$, where the samples show $\mathbf{P} \parallel \mathbf{a}$ at $H = 0$. [32]

$GdMnO_3$ also shows an incommensurate ordering (A type) of the Mn^{3+} moments at ~42 K. At 18 K, it transforms into a commensurate structure in the ab plane with a ferromagnetic component along the c axis due to the canting of the moments. At the same temperature, the Gd^{3+} moments order antiferromagnetically to the Mn^{3+} moments along the z direction.[12,38] The dissimilar behavior of $GdMnO_3$ and $TbMnO_3$ may be attributed to the interplay of two factors, (i) the value of the M-O-M bond angle and its effect on NN and NNN interactions, and (ii) the different magnetic interaction of Mn with the rare earth, $J_{Mn\text{-}R}$. It is known that Tb^{3+} shows Ising-type anisotropy while zero angular momentum Gd^{3+} behaves as a Heisenberg spin.[32]

$TbMn_{0.9}Al_{0.1}O_3$ and $GdMnO_3$ show a similar M-O-M bond angle so an incommensurate ordering of the Mn^{3+} moments is expected. However, the presence of Tb^{3+} moments with two Ising axes in the ab plane prevents the formation of the commensurate structure observed in $GdMnO_3$. Moreover, the disorder produced by Al doping impedes the occurrence of spontaneous polarization, either $\mathbf{P} \parallel \mathbf{a}$ or $\mathbf{P} \parallel \mathbf{c}$ at zero-field.

The application of a magnetic field favors metamagnetic transition of Tb^{3+} moments as well as the formation of **P** ∥ **a** for **H** ∥ **b** in both $TbMnO_3$ and $GdMnO_3$.

Surprisingly, the dilution with Al also significantly affects the ordering of the Tb^{3+} ions and its coupling with the Mn ordered sublattice. Measurements of C_p/T show a strong decrease of the peak associated with long-range magnetic order of Tb^{3+} moments for very low Al substitution. The observed magnetic ordering for Tb^{3+} is of short range and leads to the appearance of strong diffuse scattering. It has been reported that the dilution of Mn with other nonmagnetic cations is detrimental to long-range order of Tb.[17] In the present case, scans on the reciprocal lattice indicate that the ordering of Tb is incommensurate but of different nature than in $TbMnO_3$. The relationship $3q_{Tb}-q_{Mn} \sim 1$ is no longer valid for $TbMn_{0.9}Al_{0.1}O_3$. This may also be related to the absence of a long-range FE ordering in these compounds and, therefore, points to the importance of the Mn-Tb coupling in their multiferroicity.

The application of an external **H** leads to metamagnetic transitions of the Tb^{3+} moments. These transitions are clearly seen in both the hysteresis loops (Fig. 5) and in the neutron patterns. At 15 K and $H \geqslant 30$ kOe, the Tb^{3+} moments show a noncollinear arrangement of type C_xF_y. The Mn^{3+} sublattice preserves the sinusoidal ordering under these conditions; a graphical visualization of the full magnetic structure is drawn in Fig. 9(a). Below 8 K, the ordering of Tb^{3+} is of short range and the strong diffuse scattering impedes to the precise determination of the ordering type for Mn^{3+}, which is presumably sinusoidal. The diffuse contribution decreases in magnetic field due to the metamagnetic transition of Tb^{3+}. The magnetic structure at high field is again of C_xF_y type. Upon these conditions (2 K and high **H**), the refinements of magnetic satellites ascribed to the Mn ordering agree with an A-type component along the x direction suggesting a cycloid magnetic structure in the ab plane. The magnetic transition in the Mn sublattice agrees with the changes observed in Cp/T measurements for $H \geqslant 50$ kOe. The magnetic structure at 2 K and 60 kOe is shown in Fig. 9(b). It is the same as the structure found for manganites developing spontaneous polarization

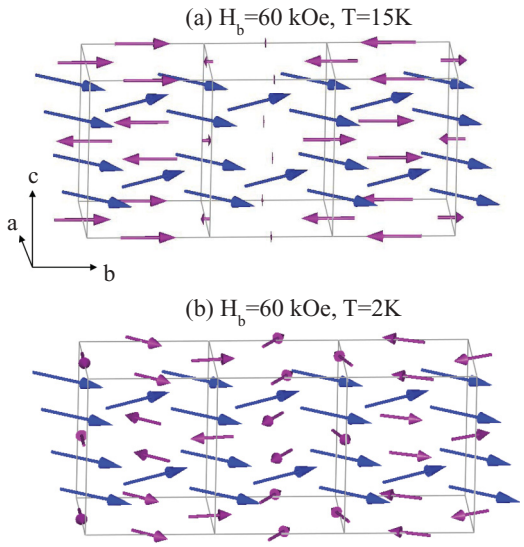

FIG. 9. (Color online) Magnetic structure of Tb^{3+} (blue arrows) and Mn^{3+} (purple arrows) moments at (a) 15 K and 60 kOe and (b) 2 K and 60 kOe.

along the a axis.[13] Therefore, our results suggest that a magnetic field (**H** ∥ **b**) induces an electric phase transition from a relaxor behavior to a ferroelectric state (**P** ∥ **a**) in $TbMn_{0.9}Al_{0.1}O_3$. Polarization measurements are desirable to confirm this point and to establish the critical field for the phase transition and its temperature evolution. Summarizing, the effects produced by the dilution of the Mn sublattice with a small isovalent nonmagnetic cation in the multiferroic $TbMnO_3$ are systematically studied, and ascribed either to magnetic dilution or structural strain.

ACKNOWLEDGMENTS

The authors thank ILL for granting beam time, especially in the Spanish CRG D15 and D1B lines. Financial support from Spanish MICINN (Projects No. FIS08-03951 and No. MAT2007-61621) and DGA (CAMRADS) is acknowledged. V.C. thanks the FPU research grant from MICINN.

*Corresponding author: Instituto de Ciencia de Materiales de Aragón, CSIC-Universidad de Zaragoza, 50009 Zaragoza (Spain); jbc@posta.unizar.es

†Present address: Centro Universitario de la Defensa, Academia General Militar, Ctra. Huesca, s/n. 50090 Zaragoza, Spain.

[1] K. Kimura, T. Goto, H. Shintani, K. Ishizka, T. Arima, and Y. Tokura, Nature (London) **426**, 55 (2003).

[2] N. Aliouane, D. N. Argyriou, J. Strempfer, I. Zegkinoglou, S. Landsgesell, and M. v. Zimmermann, Phys. Rev. B **73**, 020102(R) (2006).

[3] D. Meier, N. Aliouane, D. N. Argyriou, J. A. Mydosh, and T. Lorenz, New J. Phys. **9**, 100 (2007).

[4] N. A. Hill, J. Phys. Chem. B **104**, 6694 (2000).

[5] S. Quezel, F. Tcheou, J. Rossat-Mignod, G. Quezel, and E. Roudaut, Physica B **86**, 916 (1977).

[6] J. Blasco, C. Ritter, J. García, J. M. deTeresa, J. Pérez-Cacho, and M. R. Ibarra, Phys. Rev. B **62**, 5609 (2000).

[7] M. Kenzelmann, A. B. Harris, S. Jonas, C. Broholm, J. Schefer, S. B. Kim, C. L. Zhang, S.-W. Cheong, O. P. Vajk, and J. W. Lynn, Phys. Rev. Lett. **95**, 087206 (2005).

[8] R. Kajimoto, H. Yoshizawa, H. Shintani, T. Kimura, and Y. Tokura, Phys. Rev. B **70**, 012401 (2004).

[9] A. Muñoz, M. T. Casais, J. A. Alonso, M. J. Martínez-Lope, J. L. Martínez, and M. T. Fernández-Díaz, Inorg. Chem. **40**, 1020 (2001).

[10] O. Prokhnenko, R. Feyerherm, E. Dudzik, S. Landsgesell, N. Aliouane, L. C. Chapon, and D. N. Argyriou, Phys. Rev. Lett. **98**, 057206 (2007).

[11] O. Prokhnenko, R. Feyerherm, M. Mostovoy, N. Aliouane, E. Dudzik, A. U. B. Wolter, A. Maljuk, and D. N. Argyriou, Phys. Rev. Lett. **99**, 177206 (2007).

[12]T. Kimura, G. Lawes, T. Goto, Y. Tokura, and A. P. Ramírez, Phys. Rev. B **71**, 224425 (2005).
[13]N. Aliouane, K. Schmalzl, D. Senff, A. Maljuk, K. Prokes, M. Braden, and D. N. Argyriou, Phys. Rev. Lett. **102**, 207205 (2009).
[14]K. Noda, S. Nakamura, and H. Kuwahara, IEEE Trans. Magn. **41**, 2814 (2005).
[15]T. Kimura, S. Ishihara, H. Shintani, T. Arima, K. T. Takahashi, K. Ishizaka, and Y. Tokura, Phys. Rev. B **68**, 060403(R) (2003).
[16]M. Mochizuki and N. Furukawa, Phys. Rev. B **80**, 134416 (2009).
[17]O. Prokhnenko, N. Aliouane, R. Feyerherm, E. Dudzik, A. U. B. Wolter, A. Maljuk, K. Kiefer, and D. N. Argyriou, Phys. Rev. B **81**, 024419 (2010).
[18]V. Cuartero, J. Blasco, J. García, G. Subías, and M. C. Sánchez, J. Phys.: Conf. Series **200**, 012024 (2010).
[19]V. Cuartero, J. Blasco, J. García, G. Subías, C. Ritter, and J. A. Rodríguez-Velamazán, Phys. Rev. B **81**, 224117 (2010).
[20]R. D. Shannon, Acta Crystallogr. Sect. A **32**, 751 (1976).
[21]Y. Q. Li, N. Hirosaki, R. J. Xie, T. Takeda, S. E. Lofland, and K. V. Ramanujachary, J. Alloys Compd. **484**, 943 (2009).
[22]J. Blasco, M. C. Sánchez, J. García, J. Stankiewicz, and J. Herrero-Martín, J. Cryst. Growth **310**, 3247 (2008).
[23]J. Rodríguez-Carvajal, Physica B **192**, 55 (1993); http://www.ill.eu/sites/fullprof/.
[24]A. Bombik, B. Lesnewska, J. Mayer, and A. W. Pacyna, J. Magn. Magn. Mater. **257**, 206 (2003).
[25]J. Mareschal, J. Sivaridière, G. F. De Vries, and E. F. Bertaut, J. Appl. Phys. **39**, 1364 (1968).
[26]E. F. Bertaut, Acta Crystallogr. Sect. A **24**, 217 (1968).
[27]L. Holmes, R. Sherwood, and L. G. Van Uitert, J. Appl. Phys **39**, 1373 (1968).
[28]S. L. Gnatchenko, K. Piotrowski, A. Szewczyk, and H. Szymczak, J. Magn. Magn. Mater. **128**, 307 (1994).
[29]J. B. Gruber, K. L. Nash, R. M. Yow, D. K. Sardar, U. V. Valiev, A. A. Uzokov, and G. W. Burdick, J. Lumin. **128**, 1271 (2008).
[30]Y. Cui, Ch. Wang, and B. Cao, Solid State Commun. **133**, 641 (2005).
[31]A. M. Kadomtseva, I. B. Krynetsky, M. D. Kuz'min, and A. Z. Zvezdin, J. Magn. Magn. Mater. **81**, 196 (1989).
[32]T. Goto, Y. Yamasaki, H. Watanabe, T. Kimura, and Y. Tokura, Phys. Rev. B **72**, 220403(R) (2005).
[33]N. Aliouane, O. Prokhnenko, R. Feyerherm, M. Mostovoy, J. Strempfer, K. Habicht, K. C. Rule, E. Dudzik, A. U. B. Wolter, A. Maljuk, and D. N. Argyriou, J. Phys.: Condens. Matter **20**, 434215 (2008).
[34]J. Rodríguez-Carvajal; program available at www.ill.eu/sites/fullprof/.
[35]O. L. Makarova, I. Mirebeau, S. E. Kichanov, J. Rodríguez-Carvajal, and A. Forget, Phys. Rev. B **84**, 020408(R) (2011).
[36]V. M. Goldschmidt, *Geochemistry* (Oxford University Press, Oxford, 1958).
[37]K. Noda, S. Nakamura, J. Nagayama, and H. Kuwahara, J. Appl. Phys. **97**, 10C103 (2005).
[38]J. Hemberger, S. Lobina, H.-A. Krug von Nidda, N. Tristan, V. Yu. Ivanov, A. A. Mukhin, A. M. Balbashov, and A. Loidl, Phys. Rev. B **70**, 024414 (2004).